Critical Role of Arginine 160 of the EutB Protein Subunit for Active Site Structure and Radical Catalysis in Coenzyme B_{12}-Dependent Ethanolamine Ammonia-lyase[†]

Li Sun, Olivia A. Groover, Jeffrey M. Canfield, and Kurt Warncke*

Department of Physics, Emory University, Atlanta, Georgia 30322

Received November 30, 2007; Revised Manuscript Received March 10, 2008

ABSTRACT: The protein chemical, kinetic, and electron paramagnetic resonance (EPR) and electron spin−echo envelope modulation (ESEEM) spectroscopic properties of ethanolamine ammonia-lyase (EAL) from *Salmonella typhimurium* with site-directed mutations in a conserved arginine residue (R160) of the active site containing EutB protein subunit have been characterized. R160 was predicted by a comparative model of EutB to play a critical role in protein structure and catalysis [Sun, L., and Warncke, K. (2006) *Proteins: Struct., Funct., Bioinf. 64*, 308−319]. R160I and R160E mutants fail to assemble into an EAL oligomer that can be isolated by the standard enzyme purification procedure. The R160K and R160A mutants assemble, but R160A EAL is catalytically inactive and reacts with substrates to form magnetically isolated Co^{II} and unidentified radical species. R160A EAL activity is resurrected by externally added guanidinium to 2.3% of wild-type EAL. R160K EAL displays catalytic turnover of aminoethanol, with a 180-fold lower value of k_{cat}/K_M relative to wild-type enzyme. R160K EAL also forms Co^{II}−substrate radical pair intermediate states during turnover on aminoethanol and (*S*)-2-aminopropanol substrates. Simulations of the X-band EPR spectra show that the Co^{II}−substrate radical pair separation distances are increased by 2.1 ± 1.0 Å in R160K EAL relative to wild-type EAL, which corresponds to the predicted 1.6 Å change in arginine versus lysine side chain length. ^{14}N ESEEM from a hyperfine-coupled protein nitrogen in wild type is absent in R160K EAL, which indicates that a guanidinium ^{14}N of R160 interacts directly with the substrate radical through a hydrogen bond. ESEEM of the ^{2}H-labeled substrate radical states in wild-type and R160K EAL shows that the native separation distances among the substrate C1 and C2, and coenzyme C5′ reactant centers, are conserved in the mutant protein. The EPR and ESEEM measurements evince a protein-mediated force on the C5′-methyl center that is directed toward the reacting substrate species during the hydrogen atom transfer and radical rearrangement reactions. The results indicate that the positive charge at the residue 160 side chain terminus is required for proper folding of EutB, assembly of a stable EAL oligomer, and catalysis in the assembled oligomer.

The bacterial enzyme ethanolamine ammonia-lyase (EAL,[1] EC 4.3.1.7; also known as ethanolamine deaminase) (*1, 2*) is a coenzyme B_{12}- (adenosylcobalamin-) dependent enzyme that catalyzes the conversion of aminoethanol to acetaldehyde and ammonia (*3*) by using highly reactive radical intermediates. EAL from *Salmonella typhimurium* is composed of a 453-residue, 49.4 kDa EutB protein subunit and a 286-residue, 32.1 kDa EutC protein subunit, which are coded by the *eutb* and *eutc* genes, respectively (*4*). EutB contains the active site (*5*). The enzyme molecule has a molecular mass of approximately 500 kDa, which indicates that the two subunits are present in a $EutB_6EutC_6$ stoichiometry (*6*). The structures of several coenzyme B_{12}-dependent enzymes in cofactor-bound, diamagnetic states have been solved by X-ray crystallography (*7*−*16*). High-resolution (0.1−1.0 Å) structures of the reactant center geometries in the paramagnetic, Co^{II}−radical pair catalytic intermediate states have been determined in EAL by using techniques of electron paramagnetic resonance (EPR) spectroscopy (*17*−*21*). The structure of EutB from *Listeria monocytogenes* has been deposited in the Protein Data Bank (*22*). The coenzyme and substrate are absent in this structure (*22*). A protein context for the Co^{II}−radical pair reactant center geometries is, however, provided by a comparative model of the EutB protein from *S. typhimurium* (*5*), which includes the positions of the cofactor and bound substrate. As shown in Figure 1A,B, the polypeptide backbone and secondary structure of the $\beta_8\alpha_8$, TIM-barrel fold of EutB in the *S. typhimurium* model and *L. monocytogenes* structure display very good agreement. The EutB model was used to predict pivotal roles for the side chain of an active site arginine residue (R160) in protein structuring, substrate binding, and radical catalysis (*5*). Figure 1A,B shows that the position of the R160 side chain in the *S. typhimurium* model and *L. monocytogenes* structure is also in excellent agreement. In this report, we test the predicted roles for R160 by using techniques of site-directed mutagenesis, enzyme kinetics, and a comprehensive

[†] This work was supported by NIH Grant DK54514.

* Corresponding author. E-mail: kwarncke@physics.emory.edu. Phone: 404-727-2975. Fax: 404-727-0873.

[1] Abbreviations: EPR, electron paramagnetic resonance; ESE, electron spin−echo; ESEEM, electron spin−echo envelope modulation; ENDOR, electron−nuclear double resonance; EAL, ethanolamine ammonia-lyase; C1, carbinol carbon of substrate; C2, amino carbon of substrate; WT, wild type; SDS, sodium dodecyl sulfate; PAGE, polyacrylamide gel electrophoresis; NADH, reduced nicotinamide adenine dinucleotide.

10.1021/bi702366e CCC: $40.75
Published on Web 04/30/2008

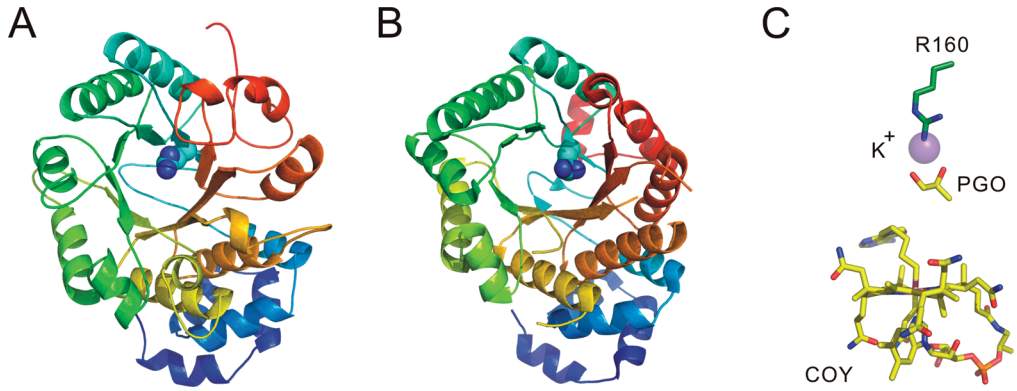

FIGURE 1: Structures of the EutB protein of ethanolamine ammonia-lyase and the position of the R160 side chain determined by comparative modeling and by X-ray crystallography. (A) Comparative model of the EutB protein from *S. typhimurium* (*5*) showing the $\beta_8\alpha_8$ region (residues 79−432). The R160 side chain is depicted in van der Waals surface mode. (B) X-ray crystallographic structure of the EutB protein (chain A) from *L. monocytogenes*, PDB accession code 2qez (*22*), showing the $\beta_8\alpha_8$ region (residues 79−432). The R160 side chain is depicted in van der Waals surface mode. (C) Relative positions of the R160 side chain, cofactor, and substrate in the active site of the comparative model of the EutB protein from *S. typhimurium* (*5*). The cofactor (COY) and substrate (PGO) positions were determined by the template−target match with the structure of the large subunit of diol dehydratase (1eex:A) (*13*). The relative position of the potassium ion (K^+) in the active site of 1eex:A (*13*) is shown by the violet van der Waals sphere. The *L. monocytogenes* 2qez EutB structure does not include the cofactor or substrate.

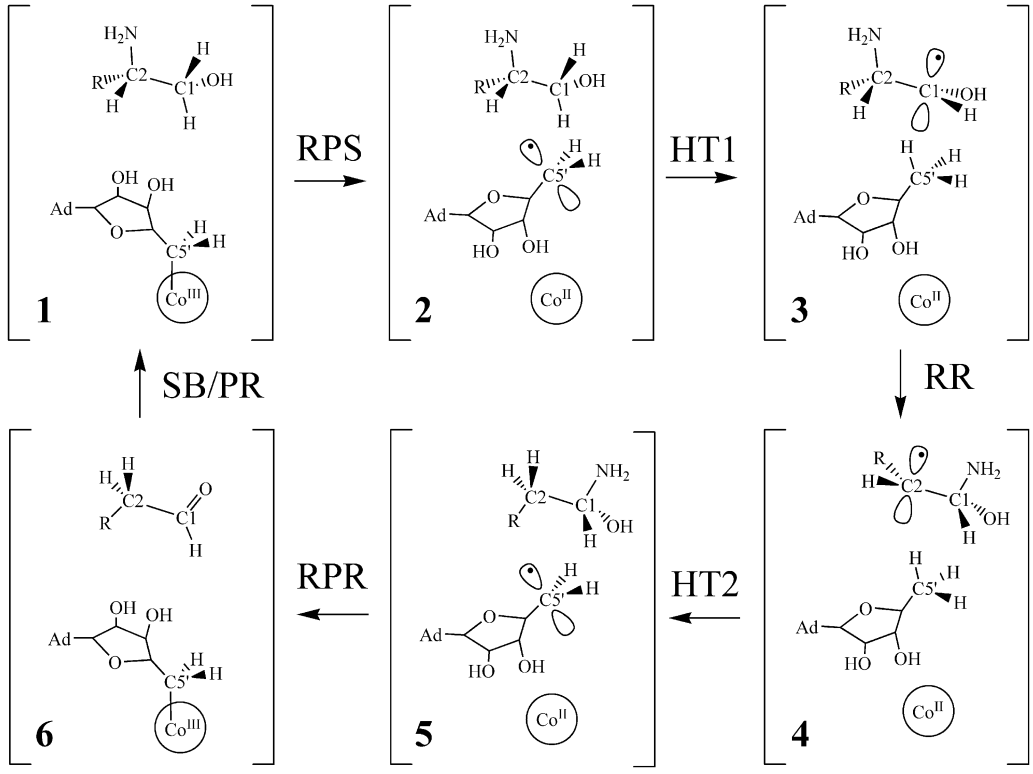

FIGURE 2: Minimal mechanism of catalysis for coenzyme B_{12}-dependent ethanolamine ammonia-lyase. The forward direction of the reaction is indicated by the arrows. Steps of the cycle are denoted RPS (radical pair separation), HT1 (first hydrogen atom transfer), RR (radical rearrangement), HT2 (second hydrogen atom transfer), RPR (radical pair recombination), and SB/PR (substrate binding/product release). The brackets represent the active site region in the protein interior. The adenine group of the 5′-deoxyadenosyl β-axial ligand is denoted as Ad. The cobalt ion and its formal oxidation states are depicted, but the corrin ring and α-axial ligand of the coenzyme are not shown. The substrates are aminoethanol (R = H) or (*S*)-2-aminopropanol (R = CH_3). The forms of the substrate are as follows: states 1 and 2, bound substrate; state 3, substrate radical; state 4, product radical; state 5, bound carbinolamine intermediate; state 6, bound aldehyde and ammonia products.

EPR spectroscopic protocol for assessing the impact of the mutations on reactant and protein structure.

Figure 2 shows the minimal catalytic mechanism proposed for EAL (*1, 2*). Following the homolytic cleavage of the metal−alkyl bond between cobalt (Co^{III}) and C5′ of the 5′-deoxyadenosyl axial ligand, the C5′ radical center migrates to the substrate binding site and abstracts a hydrogen atom from the carbinol carbon (C1) of the substrate, forming a substrate radical with unpaired electron spin density localized on C1 (*23*). The subsequent radical rearrangement reaction produces the product radical, which is predicted to be in the C1-carbinolamine form (*24, 25*), with the unpaired electron localized on C2. After the rearrangement, a hydrogen atom transfer from the 5′-methyl group of 5′-deoxyadenosine to

C2 of the product radical forms a diamagnetic product species and regenerates the 5′-deoxyadenosyl radical, which recombines with Co^{II} to complete the catalytic cycle (*26*).

In EAL, the Co^{II}−substrate radical pair intermediate accumulates during steady-state turnover on the substrates (*S*)-2-aminopropanol (*23*) and aminoethanol (*27*). These radical pair states were stably cryotrapped (*23, 28*) for investigation by different techniques of EPR spectroscopy. EPR simulations show that the Co^{II}−C1 separation is 11 ± 1 Å in the (*S*)-2-aminopropanol-generated Co^{II}−substrate radical pair (*18, 29*) and 9.3 ± 1 Å in the aminoethanol-generated Co^{II}−substrate radical pair (*21, 30*). These distances span the active site region, from the cobalamin to the substrate binding site. As shown by the approximately 2 Å shift of the C1 position in the 2-aminopropan-1-ol-1-yl radical relative to the aminoethan-1-ol-1-yl radical, which is caused by the methyl substitution at C2, the Co^{II}−C1 separation is a sensitive indicator of structural perturbations. Subangström resolution of the distances between the C1, C2, and C5′-methyl centers in the local region of the substrate binding site has been achieved by electron spin−echo envelope modulation (ESEEM) and electron−nuclear double resonance (ENDOR) spectroscopies. Multifrequency powder (*17, 20*) and orientation-selection (*18, 21*) ESEEM studies of the hyperfine interaction between the radicals and ^{2}H-labeled hydrogen sites on the C5′-methyl group of 5′-deoxyadenosine have led to a three-dimensional model of the C1, C2, and C5′-methyl group reactant center geometry in each of the Co^{II}−substrate radical pair states. ^{13}C-ENDOR results are consistent with this model (*19*). The magnetic coupling of the substrate radicals with a protein nitrogen nucleus has also been characterized by using ^{14}N ESEEM (*31, 32*). The EPR and ESEEM measurements are sensitive to structural perturbations in the active site, on length scales from 0.1 to 10 Å. Therefore, the spectroscopies are useful as probes of the effects of the site-directed mutations on the reactant center geometry and reactant−protein interactions.

Figure 1C shows the R160 side chain in the substrate binding region of the EutB model (*5*). The substrate, cofactor, and potassium ion (K^+) are from the diol dehydratase 1eex:A X-ray crystallographic structure (*13*), which was used as the template for the EutB model. The substrate and K^+ are positioned according to the template (1eex:A)−target (EutB) match, and the substrate position is consistent with the dimensions of the substrate binding cavity in EutB (*5, 22*). However, there is no evidence for protein ligands that form a K^+ binding site in EutB. Instead, the guanidinium group of R160 overlaps the van der Waals sphere of the K^+. This led us to hypothesize (*5*) that R160 organizes the protein around the substrate binding site, and that it has the same "scaffolding" function for the substrate during the rearrangement reaction that was proposed (*2, 12, 13*) for K^+ in diol dehydratase. Arginine side chains have also been proposed to position substrates for catalysis in the coenzyme B_{12}-dependent mutase enzymes (*9, 10, 33*). In addition, the guanidinium group of R160 is positioned near the migrating group, as shown in Figure 2. *Ab initio* calculations on simple model systems show that the barrier to amine migration is lowered if the migrating group is "partially protonated" during rearrangement (*34, 35*). Therefore, R160 in EutB was also proposed to accelerate the rearrangement reaction by both general acid and electrostatic catalysis (*5*).

We have characterized the protein chemical, enzyme kinetic, and EPR spectroscopic properties of EAL with mutations at position 160 of EutB (R160K, R160A, R160E, and R160I) and compared the properties with wild-type (WT) EAL. The R160I and R160E mutants fail to assemble into an EAL oligomer that can be isolated by the standard enzyme purification procedure. The R160K and R160A mutants assemble, but R160A is catalytically inactive and reacts with substrates to form uncoupled Co^{II} and unidentified protein-based radical species. R160K displays catalytic turnover of aminoethanol and the formation of Co^{II}−radical pair intermediate states. EPR and ESEEM spectroscopies and simulations reveal that the native Co^{II}−radical pair separation distances are increased by 2.1 ± 1.0 Å in R160K but that the geometry of the C1, C2, and C5′-methyl group reactant centers is conserved. The results indicate that the positive charge at the residue 160 side chain terminus is required for proper folding of EutB, assembly of a stable EAL oligomer, and catalysis in the assembled oligomer.

EXPERIMENTAL PROCEDURES

Site-Directed Mutagenesis. The 8.5 kb plasmid containing the *S. typhimurium* ethanolamine ammonia-lyase coding sequence was extracted from the *Escherichia coli* overexpression strain (*4*) with the Qiagen QIAprep spin miniprep kit (Qiagen Co., Valencia, CA). Site-directed mutagenesis was performed on the arginine 160 position within the *eutb* sequence by using the GeneTailor site-directed mutagenesis kit (Invitrogen Co., Carlsbad, CA). Five plasmids, including four mutations (R160A, R160K, R160E, and R160I) and a WT control, were constructed. Briefly, the original plasmid was first methylated with DNA methylase and amplified individually with five pairs of overlapping primers, which either contained the WT Arg160 or the four desired mutations. The list of primers used is presented in Table S1 (Supporting Information). Platinum Taq polymerase (Invitrogen Co., Carlsbad, CA) was used for the PCR reactions and followed by transformation into the competent *E. coli* DH5α $T1^R$ strain that circularizes the linear mutated DNA and digests the methylated templates. Positive transformations were selected by ampicillin resistance on LB plates. The mutations on the new plasmids were confirmed by nucleotide sequencing (performed by Cogenics Co., Morrisville, NC).

Enzyme Preparation. DH5α $T1^R$ *E. coli* strains containing expression plasmids for WT and the four mutated *eutb* were grown in a 10 L volume in a BioFlo 110 fermentor (New Brunswick Scientific Co., Inc., Edison, NJ) and harvested following standard protocols (*6*). Enzymes were purified as previously described (*6*), except that the enzymes were dialyzed against a final buffer containing 100 mM HEPES (pH 7.50), 10 mM potassium chloride, 5 mM dithiothreitol, and 10% glycerol (*36*).

Polyacrylamide Gel Electrophoresis. Polyacrylamide gel electrophoresis (PAGE) was performed under both nondenaturing conditions (*37*) and denaturing conditions (*38*), as previously described. Protein was stained by using Coomassie blue dye.

Enzyme Activity Assay. EAL enzyme activity was measured by using the coupled assay with alcohol dehydrogenase and NADH (*39*), in which oxidation of NADH,

which is proportional to the production of acetaldehyde by EAL, was monitored at $\lambda = 340$ nm. For the WT EAL, a stock of 1.25 mg/mL EAL and 30.4 μM adenosylcobalamin was first incubated at 25 °C for 15 min to ensure completion of holoenzyme formation (*40*). Alternatively, for mutant R160A and R160K EAL, the stock concentration was typically 7 mg/mL mutant EAL and 160 μM adenosylcobalamin. A 20 μL aliquot of the incubated stock was then diluted to a total volume of 500 μL with 50 mM potassium phosphate (pH 7.5) and added to a 500 μL solution containing 50 mM potassium phosphate (pH 7.5), 4.3 units/mL alcohol dehydrogenase, and a series of concentrations of aminoethanol, corresponding to approximately 0.2−10 times the value of the Michaelis constant, K_M. The reaction velocity (v) was then measured immediately by using the A_{340} value, with a conversion factor of 6.2 A_{340}/μmol of product (*39*). The maximum reaction velocity (V_{max}) and K_M were calculated from fits of Hanes−Woolf plots (*41*).

R160A Enzyme Activity Assay in the Presence of Guanidine Hydrochloride. The specific activities of R160A and WT for the substrate aminoethanol were determined in the presence of 0.1, 1.0, 10.0, and 100.0 mM guanidine hydrochloride. The enzyme activity assays were performed following the same procedure described in the enzyme activity assay section, except that the substrate concentration was 10 mM and the final concentrations of R160A and WT protein in the assay were 0.143 and 0.025 mg/mL, respectively. A guanidine hydrochloride solution was adjusted to pH 7.5 and added to the EAL and the adenosylcobalamin mixture for a 10 min preincubation, prior to addition of alcohol dehydrogenase and the substrate, aminoethanol.

EPR Sample Preparation. Aminoethanol (natural abundance, [$^1H_4$]aminoethanol) and (*S*)-2-aminopropanol (Aldrich Chemical Co., St. Louis, MO), [1,1,2,2-$^2H_4$]aminoethanol ([$^2H_4$]aminoethanol; Cambridge Isotope Laboratories, Inc.), [1,2-$^{13}C_2$]aminoethanol, [1-^{13}C]aminoethanol (Cambridge Isotope Laboratories, Inc., Andover, MA), and adenosylcobalamin (Sigma Chemical Co., St. Louis, MO) were purchased from commercial sources. Reactions were performed in air-saturated 10 mM potassium phosphate (pH = 7.5) buffer. All manipulations were performed under dim red safe lighting on ice (273 K; aminoethanol reactions) or at room temperature [295 K; (*S*)-2-aminopropanol reactions]. The concentration of wild-type and mutant ethanolamine ammonia-lyase ranged from 10 to 30 mg/mL, which is equivalent to 20−60 μM for a holoenzyme molecular mass of 500000 g/mol (*6*). Adenosylcobalamin (180−540 μM) was added to each sample to satisfy a 1.5:1 cobalamin:active site ratio. The active site:holoenzyme stoichiometry is 6 (*42, 43*). After the addition of adenosylcobalamin to the mixture of enzyme and substrate, the solution was injected into a 4 mm o.d. EPR tube, which was immersed immediately into liquid nitrogen-chilled isopentane (≈140 K) and transferred to liquid nitrogen (77 K). The total time from mixing to plunging into isopentane was less than 15 s. Excess substrate was added to ensure steady-state turnover at the time of cryotrapping, as previously described (*28, 32*).

Continuous-Wave EPR Spectroscopy. X-band continuous-wave EPR spectra were collected by using a commercial Bruker E500 EPR spectrometer equipped with a Bruker ER 049X X-band microwave bridge and an Oxford ESR 900 liquid helium cryostat and an Oxford ITC 503S temperature controller. All continuous-wave EPR spectra were obtained at 6 K.

ESEEM Spectroscopy. Pulsed-EPR experiments were performed by using a laboratory-constructed wideband pulsed-EPR spectrometer that will be described elsewhere (K. Warncke, in preparation). The reflection microwave probe (*44*) incorporates a folded half-wave resonator (*45*). By using a two-pulse ($\pi/2-\tau-\pi/2$) microwave pulse sequence (*46−48*), ESE-EPR spectra were obtained. The spectra were used to determine the magnetic field values for maximum ESE amplitudes for the ESEEM experiments. ESEEM was collected with the three-pulse ($\pi/2-\tau-\pi/2-T-\pi/2$) microwave pulse sequence (*46−48*), with microwave pulse swapping and phase cycling (*49, 50*). The τ values were selected to eliminate envelope modulation from the multitude of weakly dipolar-coupled "matrix" (*51*) protons that surround the radicals (*52, 53*). For the matrix ^{1}H, the hyperfine frequencies, ν_α and ν_β, corresponding to the α ($m_s = +1/2$) and β ($m_s = -1/2$) electron spin manifolds, respectively, both approximate the free ^{1}H frequency, ν_{1H} (13.3 MHz at 312.5 mT). Setting $\tau = n/\nu_{1H}$, where n is a positive integer, suppresses the matrix proton modulation (*52, 53*). Cosine Fourier transformation of the time domain envelope modulation generates the ESEEM frequency spectra. Envelope modulation was processed prior to Fourier transformation by dead time reconstruction and correction for any ESE envelope decay by fitting and subtracting a polynomial curve. ESEEM that was acquired with deuterated and natural abundance aminoethanol samples was divided in order to attenuate the modulation from commonly coupled nuclei (*53, 54*). All data acquisition and processing were performed with programs developed in Matlab (version 7.1; Mathworks, Natick, MA) and run on PCs with Windows XP OS or on a PC cluster with Linux OS at the Emerson Center for Scientific Computation, Emory University.

EPR Simulations. Simulations of the Co^{II}−substrate radical pair EPR spectra were carried out by using the program MENO (*55*), as implemented in Matlab with the addition of a fitting optimization algorithm (*18*). The Hamiltonian can be formulated as follows (*56*):

$$H = (\vec{\mu}_1 + \vec{\mu}_2)\cdot\vec{B}_0 - hJ\vec{S}_1\cdot\vec{S}_2 + \frac{\mu_0}{4\pi}\left[\frac{\vec{\mu}_1\cdot\vec{\mu}_2}{R^3} - \frac{3(\vec{\mu}_1\cdot\vec{R})(\vec{\mu}_2\cdot\vec{R})}{R^5}\right] + [hA_\perp(S_{1x}I_{1x} + S_{1y}I_{1y}) + A_\parallel S_{1z}I_{1z}] \quad (1)$$

where h is Planck's constant, μ_0 is the permittivity of free space, the subscripts 1 and 2 denote Co^{II} and the organic radical, respectively, $S_1 = S_2 = 1/2$, $I_1 = 7/2$, R is the electron magnetic dipole−dipole separation distance, J is the isotropic exchange coupling constant, and the A's are principal components of the axial cobalt hyperfine tensor. The electron spin magnetic moments for Co^{II} and the organic radical are given by the expression:

$$\vec{\mu}_j = \beta_e(g_{jx}S_{jx}\hat{x} + g_{jy}S_{jy}\hat{y} + g_{jz}S_{jz}\hat{z}) \quad (2)$$

The vector $\vec{R}$ from the radical toward Co^{II} is aligned with the g_z axis of Co^{II}, and the cobalt hyperfine and g principal axis systems are assumed to be coincident. The following parameters were fixed in the simulations: $g_{1x} = g_{1y} = g_\perp =$

2.26, $g_{1z} = g_{\|} = 2.0$, $g_{2xyz} = 2.0$, $A_{\perp} = 30$ MHz, and $A_{\|} = 309$ MHz (*18, 57*). The adjustable parameters in the simulation were *R*, *J*, and the anisotropic line widths for Co^{II} and the radical. A spherical average of simulated spectra at all possible magnetic field orientations, $\vec{B}_0$, gives the powder spectrum.

ESEEM Simulations. The ESEEM simulations are based on Mims' formalism (*52, 58*). The stationary-state Hamiltonian for treatment of the nuclear interactions is formulated as follows (*52, 58*):

$$H = h\vec{S}\cdot\boldsymbol{A}\cdot\vec{I} - g_n\beta_n\vec{B}_0\cdot\vec{I} + \vec{I}'\cdot\boldsymbol{Q}\cdot\vec{I}' \quad (3)$$

where β_n, $\vec{S}$, and $\vec{I}$ are the nuclear magneton, electron spin, and nuclear spin, respectively, g_n is the nuclear *g*-value, $\boldsymbol{A}$ is the hyperfine interaction tensor, and $\boldsymbol{Q}$ is the nuclear quadrupole interaction tensor. The different eigenstates for the hyperfine and nuclear quadrupole interactions are represented in eq 3 by $\vec{I}$ and $\vec{I}'$. Details of the application of this spin Hamiltonian to a weakly coupled radical pair state in EAL have been previously described (*18, 21*).

The diagonal hyperfine tensor, $\mathbf{A} = [A_{xx}, A_{yy}, A_{zz}]$, is separated into an isotropic component (A_{iso}) and an axially symmetric dipolar tensor, $[-A_{dip}, -A_{dip}, 2A_{dip}]$, where $A_{dip} = (\mu_0/4\pi)h^{-1}g_e\beta_e g_N\beta_N r_{eff}^{-3}$ and r_{eff} is the effective distance between the electron and the nuclear spins. Therefore, the hyperfine coupling tensor can be expressed by using two adjustable parameters, A_{iso} and r_{eff}. The nuclear quadrupole interaction tensor, $\boldsymbol{Q}$, is defined by the quadrupole coupling constant, e^2qQ/h, asymmetry parameter, η, and Euler angles, $[\alpha, \beta, \gamma]$, that determine the orientation of the quadrupole tensor with respect to the principal axes of the hyperfine coupling tensor. For axial symmetry of both the hyperfine and nuclear quadrupole tensors, β is the single adjustable Euler angle. When multiple nuclear spins are coupled to the unpaired electron spin, the products of the envelope modulation, taken separately for the α and β electron spin manifolds of the individual hyperfine couplings, were averaged to give the combined envelope modulation, as described (*53, 59*). A spherical average of simulated envelope modulations at all possible magnetic field orientations ($\vec{B}_0$) gives the powder spectrum.

The simulated spectra were dead time-reconstructed and Fourier transformed by using exactly the same procedure as used for the experimental data. The parameters A_{iso}, r_{eff}, e^2qQ/h, η, and the Euler angle, β, were varied to achieve the best overall fitting of the simulations to the experimental data in both time and frequency domains, as outlined in the following Fitting Procedures section. For ^2H hyperfine coupling, the ^2H e^2qQ/h and η were fixed at the characteristic values of 0.12 MHz and 0.1 (*60*), and the Euler angles were fixed as follows: $[\alpha = 0, \beta = 0, \gamma = 0]$.

For the aminoethanol-derived substrate radical samples, ESEEM was collected for samples with [$^2H_4$]aminoethanol or natural abundance [$^1H_4$]aminoethanol under identical conditions. Division of the ^2H envelope by the ^1H envelope attenuates the contributions of common coupled nuclei in the quotient ESEEM (*54, 61*). Factors that favor a dominance of the ^2H modulation in the quotient ESEEM, relative to the ^1H modulation, have been discussed (*20*). The $^2H/^1H$ quotient ESEEM and Fourier transforms were simulated by using four types of coupled ^2H, as assigned previously (*17, 18, 20, 21*).

Fitting Procedures. Simulations of EPR and ESEEM spectra were fitted to the experimental data by using the Nelder−Mead simplex direct search method (*62, 63*), as implemented in Matlab's "fminsearch" function. Optimal parameters were obtained by minimizing the mean squared deviation between simulations and the experimental data. Specifically, for continuous-wave EPR simulations, the mean squared deviations between simulations and the experimental data of both the first and second derivative spectra were calculated. The product of these two mean squared deviations was set as the objective function for optimization. For ESEEM simulations, the mean squared deviations between simulations and the experimental data in both time and frequency domain were calculated for spectra acquired with multiple τ values. Optimizations on the products of these mean squared deviations gave a globally optimal set of parameters in both time and frequency domain at different τ values. Optimizations were performed with programs developed in Matlab, as previously described (*21*).

For an optimal parameter set $\mathbf{x}^* = \{x_1^*, x_2^*, ..., x_n^*\}$, the upper bound error $\sigma_h(x_i^*)$ and lower bound error $\sigma_l(x_i^*)$ of parameter x_i^* were determined by

$$\begin{cases} f(x_1^*, ..., x_{i-1}^*, x_i^* + \sigma_h(x_i^*), x_{i+1}^*, ..., x_n^*) = f(\mathbf{x}^*) + a \\ f(x_1^*, ..., x_{i-1}^*, x_i^* - \sigma_l(x_i^*), x_{i+1}^*, ..., x_n^*) = f(\mathbf{x}^*) + a \end{cases} \quad (4)$$

where $i = 1, 2, \ldots, n$ and $f(\mathbf{x})$ is the objective function for the optimization and *a* is a threshold constant that is determined by visual scrutiny of overlaid data and simulations. The uncertainties, σ_h and σ_l, were obtained by using essentially the same algorithm as the program, MINUIT from the CERN numerical library (*64*). Specifically, with the assumption of $f(\mathbf{x})$ being at its parabolic minimum at x_i^*, σ_h and σ_l were conjectured, adjusted, and approximated according to evaluations of $f(\mathbf{x})$ at $x_i^* + \sigma_h$ and $x_i^* - \sigma_l$ in an iterative manner. This reduces the number of evaluations compared to a direct line search.

RESULTS AND DISCUSSION

Purification and Properties of the Ethanolamine Ammonia-lyase Protein. Purification of WT, R160A, R160K, R160I, and R160E EAL was performed by using the standard procedure (*6*). SDS−PAGE of samples from individual steps of the purification procedure showed that the R160I and R160E protein pelleted with the cell debris upon centrifugation, following cell breakage. Therefore, the R160I and R160E proteins aggregate during expression and probably form insoluble inclusion bodies. Complete purification, with protein yields comparable with WT, was achieved for R160A and R160K EAL. SDS−PAGE gels of the WT, R160A, and R160K EAL are presented in Figure 3. Figure 3 shows that the EutB band is less dense for R160A than for WT or R160K EAL and that the residual density is found in a high molecular mass band. Therefore, R160A EutB is unstable and forms strongly associated, high molecular mass aggregates. The mechanism of the protein aggregation is not known. The nondenaturing polyacrylamide gels in Figure 4 show that the R160K and R160A EutB assemble into the native oligomeric structure. Inspection of the overloaded R160A lane shows heterogeneity in the relative mobility, which suggests that the instability of R160A is associated with a less discrete structure.

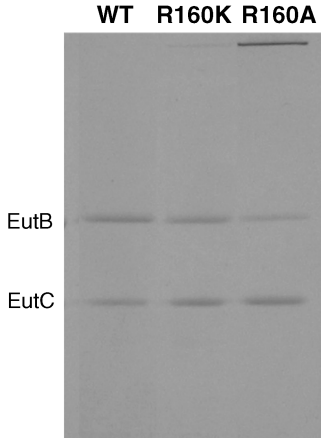

FIGURE 3: Sodium dodecyl sulfate−polyacrylamide gel electrophoresis (SDS−PAGE) gel of purified wild-type, R160K, and R160A ethanolamine ammonia-lyase. The 10% polyacrylamide gel was stained with Coomassie blue. The bands for EutB and EutC are indicated.

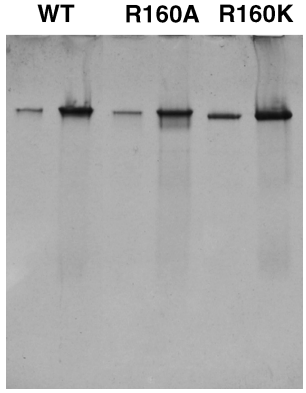

FIGURE 4: Nondenaturing polyacrylamide gel electrophoresis gel of purified wild-type, R160A, and R160K ethanolamine ammonia-lyase. The 8% polyacrylamide gel was stained with Coomassie blue. Lanes for the wild-type (WT), R160A, and R160K EAL are indicated. The left and right lanes for each protein molecule correspond to 10 g and 20 μg of protein, respectively.

The impact of the mutations on EutB folding and EAL oligomer assembly can be qualitatively rationalized, as follows. The R160 side chain is buried in the protein at the active site (*5, 22*). The polar microenvironment around R160 indicates that the side chain will be in the guanidinium form (*5, 22*). This is supported by a study of amino acid side chain ionization in proteins, which predicts that arginine in the buried and deeply buried sites in proteins is ionized with 94% and 86% probabilities, respectively (*65*). Replacing the arginine side chain with the isobutyl side chain of isoleucine in R160I EutB will therefore result in a significant Coulombic destabilization of the folded EutB state. The β-branching of isoleucine may also place additional conformational constraints on folding, relative to arginine. The nonionized side chain of glutamic acid in R160E EAL may produce a similar significant Coulombic destabilization. It is unlikely that the negatively charged carboxylate moiety would be stable in folded EutB, and it may stabilize the unfolded state relative to the folded state. Replacing R160 with alanine, which has the small methyl side chain, may allow water molecules to partially compensate for the loss of the arginine side chain. For a given conformation of their *n*-alkyl moieties, the *n*-butylamine side chain of lysine is shorter than the *n*-propylguanidine side chain of arginine by 1.6 Å. Therefore, the R160K mutation is reasonably conservative with respect to volume and local hydrophobicity. In addition, *in situ* protonation of the lysine amino group to create the ammonium charge center would contribute charge and polar interactions characteristic of the guanidinium group. The R160K mutation therefore maintains the structural integrity of EutB, leading to correct assembly of a stable EAL oligomer.

Table 1: Steady-State Enzyme Kinetic Parameters for Wild-Type and Mutant Ethanolamine Ammonia-lyase for Ethanolamine as Substrate

enzyme	K_M (μM)	k_{cat} (s^{-1})	k_{cat}/K_M ($M^{-1}\cdot s^{-1}$)
WT	13.6 ± 2.9	52.2 ± 3.7	$(3.8 \pm 1.1) \times 10^6$
R160K	410 ± 50	8.5 ± 0.6	$(2.1 \pm 0.2) \times 10^4$
R160A		$<10^{-5}$	

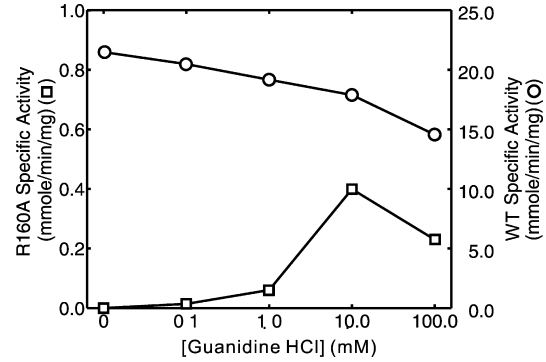

FIGURE 5: Specific activity of wild-type and R160A EAL as a function of guanidine hydrochloride concentration. The specific activities of wild-type and R160A EAL are plotted on different scales, as indicated on the right and left ordinate axes, respectively.

Enzyme Kinetic Properties of WT, R160K, and R160A EAL. Enzyme activity assays were carried out on WT, R160A, and R160K EAL with aminoethanol as substrate. Table 1 summarizes the results. R160K EAL shows a 30-fold increase in K_M for aminoethanol relative to WT enzyme. This suggests that the affinity of substrate for EAL is weakened in R160K relative to WT.

Table 1 also shows that k_{cat} for [^{1}H]aminoethanol is decreased by 6.1-fold for R160K relative to WT. R160A displays no detectable catalytic turnover with aminoethanol ($k_{cat} < 10^{-5}$ s^{-1}). The value of the specificity constant (*66*), k_{cat}/K_M, is therefore decreased by 180-fold in R160K EAL relative to WT. The results show that replacement of the native positively charged guanidinium side chain with the 1.6 Å shorter, positively charged ammonium side chain of R160K leads to a modest decrease in catalytic performance. However, removal of the molecular volume and positive charge of the arginine side chain eliminates catalysis in EAL.

Resurrection of Enzyme Activity in R160A with Externally Added Guanidine Hydrochloride. Figure 5 shows that externally added guanidine hydrochloride (HCl) leads to significant R160A EAL enzyme activity under V_{max} conditions. As shown in Figure 5, the activity of R160A EAL increases with guanidine hydrochloride concentration and reaches a maximum at 10 mM, which represents 2.3% of the activity of the WT EAL control. The structure of the guanidinium ion resembles the guanidinium group at the terminus of the arginine side chain. The results in Figure 5 indicate that the externally added guanidinium binds in the

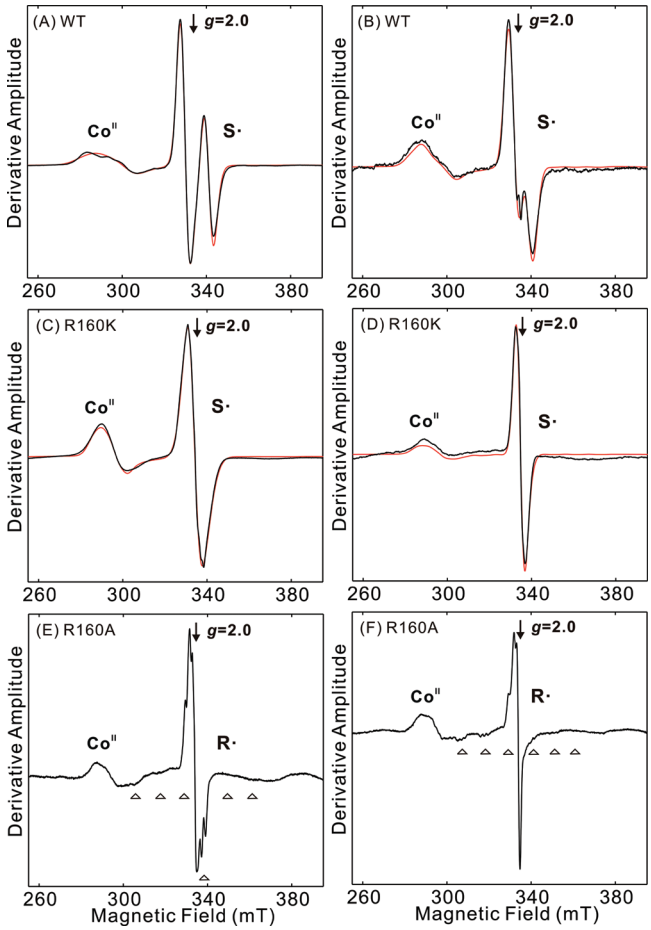

FIGURE 6: Continuous-wave EPR spectra of the cryotrapped Co^{II}−substrate radical pair and Co^{II}/radical states formed in wild-type, R160K, and R160A ethanolamine ammonia-lyase and overlaid EPR simulations (red) for wild-type and R160K EAL. The free electron resonance position at $g = 2.0$ is indicated by downward arrows. The maximum amplitude of transitions associated with Co^{II} at $g_\perp$, the substrate radical ($S^\bullet$), and the unassigned radical ($R^\bullet$) are designated. In (E) and (F), six of the eight cobalt hyperfine coupling features at $g_{||}$ are resolved and are indicated by triangles. (A) Wild-type EAL, substrate (*S*)-2-aminopropanol. (B) Wild-type EAL, substrate aminoethanol. (C) R160K EAL, substrate (*S*)-2-aminopropanol. (D) R160K EAL, substrate aminoethanol. (E) R160A EAL, substrate (*S*)-2-aminopropanol. (F) R160A EAL, substrate aminoethanol. Experimental conditions: microwave frequency, 9.348 GHz; temperature, 6 K; microwave power, 2 mW; magnetic field modulation, 1 mT; modulation frequency, 100 kHz; scan rate, 7.15 mT/s; time constant, 2.56 ms; number of averaged scans, (A−D) 32 scans, (E) 128 scans, and (F) 64 scans. An average of 128 baseline scans have been subtracted from all spectra. Simulation parameters are listed in Table 2 and Table S2 (Supporting Information).

vacant region of the arginine side chain terminus that is created by the alanine mutation in the active site of EutB. The resurrection of enzyme activity in R160A EAL by externally added guanidine hydrochloride provides strong support that a positively charged arginine side chain in the active site is catalytically essential.

EPR Spectroscopy of Co^{II} and Radicals in WT, R160K, and R160A EAL. (A) (S)-2-Aminopropanol-Generated Co^{II}-Radical Pairs. Figure 6A shows the EPR spectrum of the cryotrapped Co^{II}−substrate radical pair catalytic intermediate in WT EAL, which is formed during steady-state turnover on (*S*)-2-aminopropanol (*23*). The Co^{II} intensity is most

Table 2: EPR Simulation Parameters for the Co^{II}−Substrate Radical Pairs in Wild-Type and R160K Ethanolamine Ammonia-lyase

enzyme	substrate	parameter	best-fit value	lower bound	upper bound
WT	2-aminopropanol	*J* (MHz)	−291.2	−294.2	−288.3
		R (Å)	11.2	11.0	11.7
	1,1,2,2-$^2H_4$-aminoethanol	*J* (MHz)	−160.4	−166.5	−153.9
		R (Å)	9.4	8.6	9.8
R160K	2-aminopropanol	*J* (MHz)	−79.4	−83.2	−74.9
		R (Å)	13.3	12.3	14.41
	1,1,2,2-$^2H_4$-aminoethanol	*J* (MHz)	37.7	21.5	48.1
		R (Å)	11.5	10.0	11.7

prominent in the region around 285 mT, which is near the $g_\perp = 2.26$ value of the Co^{II} line shape in the EPR spectrum of magnetically isolated cob(II)alamin (*57*). The Co^{II} features in the radical pair spectrum are inhomogeneously broadened, relative to isolated cob(II)alamin, by the interaction with the substrate radical (*56, 57, 67*). The substrate radical line shape extends from approximately 325.0 to 345.0 mT. The doublet splitting of the substrate radical line shape is caused by the interaction with the unpaired electron spin on Co^{II} (*56, 57, 67*). The simulation of the WT EPR spectrum is shown as the red curve in Figure 6A. The EPR simulation parameters for the electron−electron separation distance (*R*) and isotropic exchange interaction (*J*) are presented in Table 2. Additional simulation parameters are presented in Table S2 (Supporting Information). The best-fit value for the separation distance between Co^{II} and the C1 radical center of the substrate radical is 11.2 Å, and the isotropic exchange coupling is −290 MHz (corresponding to antiferromagnetic coupling in the ground state), which are consistent with values previously reported (*18, 29*).

Figure 6C shows the EPR spectrum of the cryotrapped Co^{II}-radical pair formed during steady-state turnover of R160K EAL on (*S*)-2-aminopropanol. An excellent simulation of the EPR spectrum is achieved by using the best-fit parameters, $R = 13.3$ Å and $J = -79$ MHz (Table 2). The value of *J* and the absence of resolved Co^{II} hyperfine and ^{14}N axial ligand superhyperfine features in the spectrum show that Co^{II} and the radical center are electronically coupled in the R160K mutant, although the weaker coupling leads to a narrowing of the Co^{II} and radical line widths, relative to WT. The Co^{II}-radical separation is increased by 2.1 ± 0.6 Å in R160K EAL, relative to WT.

Figure 6E shows that the Co^{II} and radical features of the EPR spectrum of the cryotrapped Co^{II}-radical pair formed during steady-state turnover of R160A EAL on (*S*)-2-aminopropanol are further narrowed relative to R160K. The Co^{II} line shape shows six of the eight features that arise from the octet splitting at $g_{||}$ that arises from the cobalt hyperfine interaction ($I_{Co} = {}^7/_2$), and each feature is further split into a triplet by the superhyperfine interaction with the proximal ^{14}N ($I_N = 1$) of the dimethylbenzimidazole axial ligand (*57*). The presence of resolved cobalt hyperfine and proximal nitrogen superhyperfine features is characteristic of magnetically isolated cob(II)alamin. This suggests that the Co^{II} and radical species are separated by >14 Å.

(B) Aminoethanol-Generated Co^{II}−Substrate Radical Pair States. Figure 7A shows the EPR spectra of the Co^{II}−substrate radical pair generated by using natural abundance, [1-^{13}C]-, and [1,2-$^{13}C_2$]aminoethanols in WT EAL. The ^{13}C-label replaces diamagnetic ^{12}C with the $I = {}^1/_2$ ^{13}C nucleus

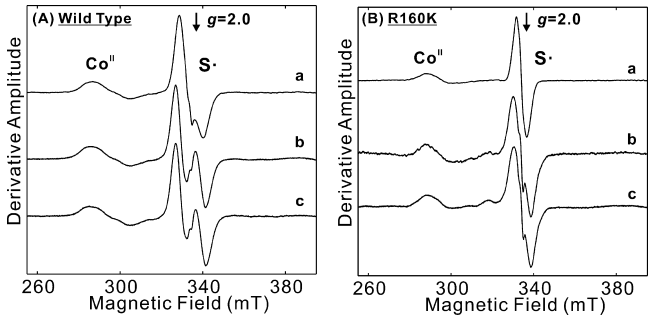

FIGURE 7: Continuous-wave EPR spectra of the cryotrapped Co^{II}−substrate radical pair states formed in wild-type and R160K ethanolamine ammonia-lyase during reaction with natural abundance and ^{13}C-labeled aminoethanols. The arrow indicates $g = 2.0$. (A) Wild-type EAL. (a) Natural abundance aminoethanol. (b) [1-^{13}C]Aminoethanol. (c) [1,2-$^{13}C_2$]Aminoethanol. (B) R160K EAL. (a) Natural abundance aminoethanol. (b) [1-^{13}C]Aminoethanol. (c) [1,2-$^{13}C_2$]Aminoethanol. Experimental conditions: microwave frequency, 9.348 GHz; temperature, 6 K; microwave power, 2 mW; magnetic field modulation, 1 mT; modulation frequency, 100 kHz; scan rate, 7.15 mT/s; time constant, 2.56 ms. All spectra are averages of 64 scans, subtracted by the average of 128 baseline scans.

and produces EPR line broadening when the unpaired electron spin is localized on the labeled carbon (*68*). The EPR spectra of the cryotrapped Co^{II}-radical pairs formed during steady-state turnover of R160K EAL on natural abundance and ^{13}C-labeled aminoethanols are shown in Figure 7B. The line widths of the radicals in R160K EAL are narrowed relative to WT, but the increase in line width for the ^{13}C-labeled radicals and the identical line width for the 1-^{13}C- and 1,2-$^{13}C_2$-labeled radicals follow the same pattern observed for WT (*28*). Therefore, as in WT, the aminoethanol-generated radical in R160K is the C1-centered substrate radical.

Figure 6B shows the EPR spectrum of the cryotrapped Co^{II}−substrate radical pair catalytic intermediate in WT EAL, which is formed during steady-state turnover on [$^2H_4$]aminoethanol (*28*). EPR simulation of the radical pair spectrum gives best-fit values of $R = 9.4$ Å for the Co^{II}−C1 separation distance and $J = -160$ MHz (Table 2; additional simulation parameters are included in Table S2, Supporting Information) for the Co^{II}−substrate radical intermediate in WT EAL, as previously reported (*21, 30*). Figure 6D shows the EPR spectrum and overlaid simulation for the aminoethanol-generated Co^{II}−substrate radical in R160K EAL. The R160K spectrum simulation shows a best-fit Co^{II}−C1 separation distance of $R = 11.5$ Å and $J = 38$ MHz (Table 2). Comparison with the R value for WT EAL indicates that the R160K mutation causes the radical center to shift 2.1 ± 1.2 Å away from Co^{II}.

The EPR spectrum of the cryotrapped paramagnetic state formed after reaction of R160A EAL with aminoethanol is shown in Figure 6F. As observed for the reaction of 2-aminopropanol with R160A, the EPR spectrum shows a narrow line radical and cobalt hyperfine and axial ligand nitrogen superhyperfine features that are characteristic of uncoupled cob(II)alamin (*57*). The origin of the radical in the R160A EAL radical was addressed by comparing the line shapes of the radical formed from [$^1H_4$]- and [$^2H_4$]aminoethanol. The ^2H-labels at C1 and C2 cause narrowing of the substrate radical line shape (*23, 28*), because the 6.51-fold smaller magnetic dipole moment of deuterium relative to protium causes a corresponding decrease in the hyperfine coupling constant. In addition, reaction of R160A EAL with [$^2H_4$]aminoethanol may result in the incorporation of one or more ^2H into the C5′-methyl group hydrogen positions (*69*). If the R160A radical resides on C1, C2, or C5′, a narrowing of the line shape is expected. It is observed that substitution of deuterium on aminoethanol does not influence the EPR line shape of the radical in R160A EAL (data not shown). The radical formed in R160A EAL is therefore not associated with the substrate or with the C5′ center.

The EPR spectroscopic results for R160A EAL are consistent with the absence of detectable turnover in this mutant. The substitution of alanine at R160 causes a mechanism-based inactivation of the enzyme, prior to completion of the full catalytic cycle. The radicals formed upon reaction with both (*S*)-2-aminopropanol and aminoethanol in R160A appear to arise from a site (or multiple sites) on the protein, which is ≥14 Å from Co^{II}.

(C) Comparison of Co^{II}−Substrate Radical Pair Separation Distances in WT and R160K EAL. The increase in Co^{II}-radical pair separation distance of 2.1 ± 0.6 and 2.1 ± 1.2 Å for the (*S*)-2-aminopropanol- and aminoethanol-derived radical pair states, respectively, is the same within the uncertainty. The distance increase is comparable to the predicted ∼1.6 Å shortening of the side chain and, therefore, of the corresponding positional shift in the positive charge center of residue 160 when lysine is substituted for arginine. As shown in Figure 1, the comparative model of EutB predicts that the guanidinium group of R160 is positioned directly over the substrate, on the side opposite Co^{II} in cobalamin (*5*). Therefore, the EPR results suggest that the substitution of the shorter lysine side chain at R160 results in an *en bloc* movement of C1 of the substrate toward the side chain terminus, which corresponds to movement away from Co^{II}.

ESEEM Spectroscopy. (A) ^{14}N ESEEM of the Substrate Radical in WT and R160K EAL. The hyperfine coupling of the unpaired electron spin on C1 of the substrate radicals with a ^{14}N nucleus on the protein was previously characterized by using ^{14}N ESEEM spectroscopy (*31, 32*). This coupling provides a sensitive probe of the radical−protein interaction. Figure 8 shows the three-pulse ESEEM and Fourier transforms for the (*S*)-2-aminopropanol-generated Co^{II}−substrate radical pair in WT and R160K EAL that were obtained for τ values of 152 and 304 ns. Comparable ^{14}N ESEEM is observed from the aminoethanol-generated Co^{II}−substrate radical pair (Figure S1, Supporting Information), but at significantly lower signal-to-noise ratios, because of the lower fraction of the Co^{II}−substrate radical pair intermediate that accumulates during steady-state turnover on aminoethanol [10−20% (*28*)], relative to (*S*)-2-aminopropanol [100% (*40*)] (*32*). The ESEEM frequency spectra from WT EAL in Figure 8 show the characteristic pattern of four features observed previously (*31, 32*). The 0.8−1.0, 1.7−2.0, and 2.9−3.0 MHz features were assigned to the "hyperfine-adulterated" (*70*) ν_0, ν_-, and ν_+ nuclear quadrupole frequencies of ^{14}N, and the feature at 4.0 MHz was assigned to the $\Delta m_I = \pm 2$ splitting in the m_s manifold in which the hyperfine and nuclear Zeeman terms are additive (*31, 32*). This distinctive pattern of features arises from

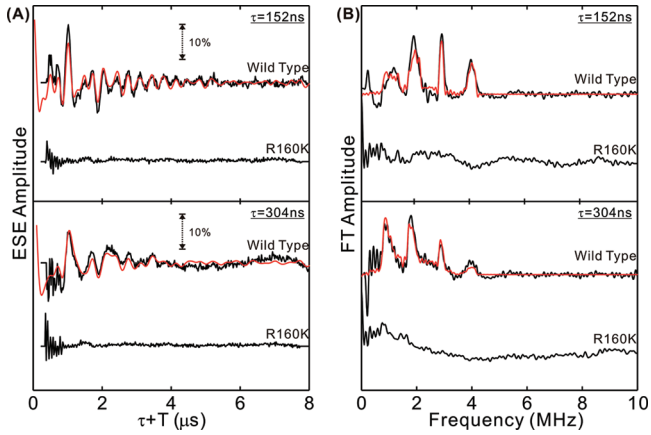

FIGURE 8: Three-pulse ESEEM and Fourier transforms for the (*S*)-2-aminopropanol-derived substrate radical in the cryotrapped Co^{II}−substrate radical pair state in wild-type and R160K ethanolamine ammonia-lyase and overlaid ^{14}N ESEEM simulations (red) for wild type. (A) ESEEM waveforms for wild-type and R160K EAL at τ values of 152 and 304 ns. The wild-type and R160K ESEEM are normalized to the unmodulated echo amplitude. The scale bar represents 10% of the total unmodulated ESE amplitude. (B) Fourier transformations of the corresponding ESEEM in (A). The frequency spectra are normalized to match the common noise level in each spectrum. Experimental conditions: temperature, 6 K; magnetic field, 309.0 mT; microwave frequency, 8.772 GHz; microwave power, 20 W; τ values, 152 and 304 ns; initial $\tau + T$ value, 120 ns; T increment, 20 ns; $\pi/2$ pulse width, 20 ns; pulse repetition rate, 100 Hz; 128 repetitions averaged per point. Simulation parameters are presented in Table 3.

Table 3: ^{14}N ESEEM Simulation Parameters for the Nitrogen Nucleus Coupled to the Substrate Radical in Wild-Type Ethanolamine Ammonia-lyase Obtained by Global Optimization of $\tau = 152$ and $\tau = 304$ ns Conditions

parameter	best-fit value	lower bound	upper bound
A_{iso} (MHz)	0.93	0.86	0.98
r_{eff} (Å)	3.42	3.14	3.46
e^2qQ/h (MHz)	3.09	3.05	3.14
η	0.55	0.51	0.58

the condition of "exact cancellation", in which the hyperfine and nuclear Zeeman contributions to the electron−^{14}N coupling cancel ($A/2 \approx \nu_N$, where A is the hyperfine coupling constant and ν_N is the free ^{14}N frequency) for one m_s manifold (*70, 71*). The ^{14}N ESEEM simulations, shown as overlaid red lines in Figure 8, reveal a nuclear quadrupole coupling constant (e^2qQ/h) of 3.09 MHz and an electric field gradient asymmetry parameter (η) of 0.55, in agreement with previous simulations (*32*). Comparable values of $e^2qQ/h = 3.19$ MHz and $\eta = 0.51$ are obtained for the aminoethanol substrate radical in WT EAL. The simulation parameters are listed in Table 3. In dramatic contrast to WT EAL, Figure 8 shows that there is no significant ESEEM signal from the Co^{II}−substrate radical in R160K EAL at $\tau = 152$ and 304 ns.

The coupled ^{14}N ESEEM nucleus was originally assigned to a peptide secondary amide nitrogen (*31, 32*), based on comparison of the ν_0, ν_-, and ν_+ values (*31*) or correspondence of the simulated $e^2qQ/h$and η values (*32*) with nuclear quadrupole double resonance parameters reported for peptide nitrogen in di- and tripeptides (*72*). The loss of the ^{14}N ESEEM in R160K EAL suggests that the arginine guanidinium group harbors the coupled nitrogen nucleus. There appear to be no reported ^{14}N nuclear quadrupole

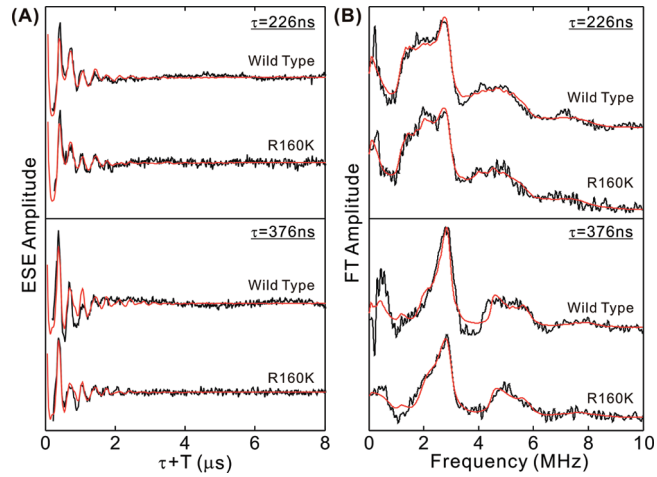

FIGURE 9: Three-pulse $^2H/^1H$ quotient ESEEM and corresponding Fourier transforms for the aminoethanol-derived substrate radical in the cryotrapped Co^{II}−substrate radical pair state in wild-type and R160K ethanolamine ammonia-lyase and overlaid ^2H ESEEM simulations (red). (A) ESEEM waveforms for wild-type and R160K EAL at τ values of 226 and 376 ns. The wild-type and R160K ESEEM is normalized to the unmodulated echo amplitude. (B) Fourier transformations of the corresponding ESEEM in (A). The frequency spectra are normalized to match the common noise level in each spectrum. Experimental conditions: temperature, 6 K; magnetic field, 312.0 mT (wild type) and 312.8 mT (R160K); microwave frequency, 8.7720 GHz; microwave power, 20−35 W; τ values, 226 and 376 ns; initial $\tau + T$ value, 120 ns; T increment, 20 ns; $\pi/2$ pulse width, 20 ns; pulse repetition rate, 200 Hz; 1280 repetitions averaged per point. Simulation parameters are presented in Table 4.

Table 4: ESEEM Simulation Parameters for the Deuterium Hyperfine Coupling in Wild-Type and R160K Ethanolamine Ammonia-lyase Obtained by Global Optimization of the $^2H/^1H$ Quotient ESEEM for $\tau = 226$ and $\tau = 376$ ns Conditions

enzyme	^2H coupling	parameter	best-fit value	lower bound	upper bound
wild type	$^2H_1$	A_{iso} (MHz)	−0.38	−0.40	−0.13
		r_{eff} (Å)	2.08	2.07	2.14
	$^2H_2$	A_{iso} (MHz)	−1.18	−1.21	−0.92
		r_{eff} (Å)	2.57	2.47	2.62
	$^2H_3$	A_{iso} (MHz)	−1.15	−1.20	−0.99
		r_{eff} (Å)	2.43	2.28	2.46
	$^2H_{\beta a}$	A_{iso} (MHz)	5.33	4.39	5.37
		r_{eff} (Å)	2.72	2.28	2.79
R160K	$^2H_1$	A_{iso} (MHz)	−0.35	−0.55	−0.06
		r_{eff} (Å)	2.10	2.07	2.20
	$^2H_2$	A_{iso} (MHz)	−1.11	−1.23	−0.90
		r_{eff} (Å)	2.45	2.37	2.66
	$^2H_3$	A_{iso} (MHz)	−1.11	−1.31	−0.66
		r_{eff} (Å)	2.45	2.28	2.73
	$^2H_{\beta a}$	A_{iso} (MHz)	5.33	5.04	5.68
		r_{eff} (Å)	2.72	2.45	3.14

parameters for arginine for comparison, but values of $e^2qQ/h = 3.48$ MHz and $\eta = 0.40$ have been reported for guanidine hydrochloride (*73*). The reported value of e^2qQ/h for guanidinium is higher than the value of $e^2qQ/h = 3.09-3.19$ MHz for the ^{14}N ESEEM nucleus in WT EAL. However, different carbon−nitrogen bond orders, and hence different electronic environments for the nitrogens in the arginine guanidinium group of R160, could arise from hydrogen bond interactions with the substrate and the asymmetric protein environment. We therefore propose that the ^{14}N ESEEM in WT EAL arises from coupling to one of the two terminal guanidinium nitrogens in the side chain of R160 from EutB.

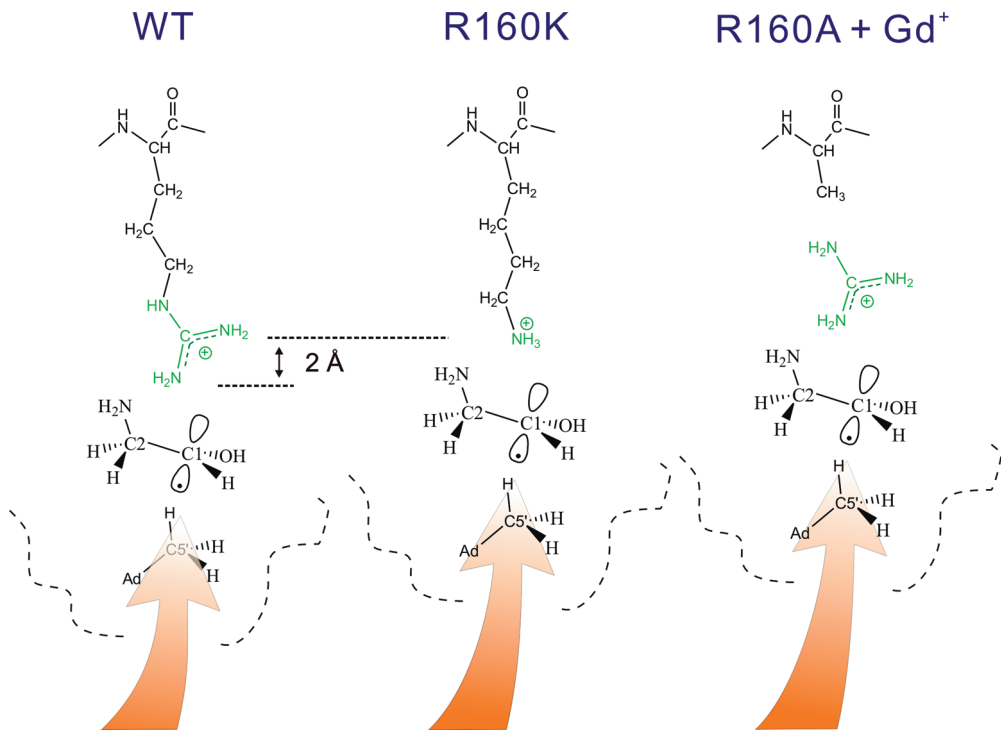

FIGURE 10: Model for the substrate binding region of the active site in WT, R160K, and R160A EAL with bound guanidinium and depiction of effects of mutations on structure. The predicted 1.6 Å difference in side chain length between arginine and lysine and the corresponding 2.1 Å displacement of the substrate and C5′ center are shown. Guanidinium is predicted to bind in the cavity created by removal of the native *n*-propylguanidinium side chain in R160A EAL. The direction of the protein-mediated force that maintains the C5′ center and substrate at van der Waals contact is depicted by the arrow.

This interaction is absent in R160K EAL, which is consistent with the structure of EutB (*5, 22*). The absence of any detectable ^{14}N ESEEM in R160K EAL suggests that the sensitive condition of "exact cancellation" (*70, 71*) is not met, which is consistent with a displacement of the lysine ammonium nitrogen relative to the guanidinium nitrogen.

(B) ^{2}H ESEEM of the Aminoethanol-Generated Radical in WT and R160K EAL. The hyperfine interaction of the unpaired electron spin at C1 of the substrate radical with ^{2}H nuclei in the C5′-methyl group provides a sensitive probe of the in situ reactant geometry at the substrate binding site (*17, 18, 20, 21*). The ^{2}H are incorporated into the C5′-methyl group by turnover of EAL on [1,1,2,2-^{2}H$_4$]aminoethanol, prior to cryotrapping (*43*). The ^{2}H-labeled aminoethanol also allows measurement of the hyperfine coupling between the unpaired electron at C1 and the β-^{2}H positions on C2. Figure 9 shows representative three-pulse ^{2}H/^{1}H quotient ESEEM for the [^{2}H$_4$]aminoethanol-generated substrate radicals in WT and R160K EAL that was collected at the maximum echo amplitude (g = 2.009). Division of the echo envelopes for ^{2}H-labeled and natural abundance (^{1}H) samples to produce the ^{2}H/^{1}H quotient ESEEM eliminates or strongly attenuates the contribution of common coupled nuclei (*53, 54*). The ^{2}H ESEEM and the corresponding Fourier transforms shown in Figure 9 for WT and R160K EAL show a high degree of similarity. The Fourier transforms in Figure 9 for τ values of 226 and 376 ns show the same features as previously reported for a different set of τ values (*20*). The broad feature at 1.0−3.0 MHz arises from coupling to one short-distance (effective electron−nuclear separation distance, r_{eff} = 2.1 Å) ^{2}H nucleus and two ^{2}H nuclei at longer separation distances (r_{eff} = 2.4−2.6 Å). The feature at 4.5−6.0 MHz in the ESEEM frequency spectrum arises from one of the two β-^{2}H hyperfine couplings ($^2H_{\beta b}$). Features from the second, more strongly coupled β-^{2}H ($^2H_{\beta b}$) are clearly observed in ESEEM experiments performed at higher resonant microwave frequency/magnetic field values (10.89 GHz/388.0 mT) but are within the noise level at 8.7−8.9 GHz/ 300.0−310.0 mT (*20*). Therefore, the ESEEM results presented in Figure 9 show that the same complement of ^{2}H is comparably coupled to the radical in WT and R160K EAL.

ESEEM simulations for the combination of ^{2}H hyperfine couplings in WT and R160K EAL are shown as the overlaid red curves in Figure 9, and the best-fit parameter values are presented in Table 4. The r_{eff} and A_{iso} values for the three C5′-methyl ^{2}H are conserved for WT and R160K EAL. The A_{iso} values of the $^2H_{\beta a}$ coupling in WT and R160K are also comparable. The A_{iso} value for $^2H_{\beta a}$ is related to the dihedral angle (θ) between the C2−$^2H_{\beta a}$ bonding orbital and the p orbital on C1 that contains the unpaired electron spin density, as follows (*74*): $A_{iso} = \rho B_2 \cos^2 \theta$, where ρ is the unpaired electron spin density on C2 and B_2 = 24.99 MHz for ^{2}H. Therefore, the C1−C2 rotamer states in WT and R160K are comparable. Overall, the ^{2}H ESEEM results indicate that the geometry of the C2, C1, and C5′-methyl centers in WT EAL is conserved in the substrate binding region of the active site in R160K EAL.

CONCLUSIONS

The principal conclusions from the protein chemical, enzyme kinetic, and EPR spectroscopic studies of the EutB R160 mutations, and their implications for factors that

determine the structure and function of EAL, are depicted in Figure 10 and summarized as follows:

(1) The positive charge at the terminus of the R160 side chain of EutB is required to achieve the native EutB protein fold and the oligomeric structure of EAL. Mutations R160E and R160I do not assemble into an oligomer. R160A EAL assembles but is unstable. The R160K mutation, which is predicted to maintain the positive charge at a similar position in the interior of EutB, leads to proper folding of EutB and assembly of a stable EAL oligomer.

(2) The positive charge at the terminus of the R160 side chain is critical for catalysis in EAL. The R160K mutation, which is predicted to maintain the positive charge at a similar position in the active site of EutB, affords turnover of aminoethanol with a relatively modest decrement of 180-fold in k_{cat}/K_M, relative to WT EAL. In addition to executing complete turnover, R160K EAL displays magnetically coupled, Co^{II}−substrate radical pair states, which are a signature of functional intermediates in EAL (*23, 28*) and other coenzyme B_{12}-dependent enzymes (*67*). In contrast, R160A EAL is inactive and forms magnetically isolated Co^{II} and radical species. The positive charge of the guanidinium group therefore appears to be the primary feature of the R160 side chain that is most essential to catalysis, followed by the capability to form hydrogen bonds with the reactant species.

(3) The R160 side chain directly interacts with the substrate species through a hydrogen bond. This conclusion is based on the proposal that the ^{14}N nuclear quadrupole parameters ($e^2qQ/h = 3.09$ MHz, $\eta = 0.5$) from the ESEEM simulations correspond to an amide-like guanidinium nitrogen. The significant A_{iso} value from the ESEEM simulations indicates a through-bond transmission of unpaired electron spin density to the ^{14}N nucleus. A minimum through-bond pathway from the C1 spin density center to a guanidinium nitrogen that is hydrogen bonded to the carbinol oxygen would involve two covalent bonds and one hydrogen bond. This is similar to the path length for the classical case of exact cancelation ^{14}N ESEEM from coupling to the remote nitrogen of imidazole in Cu^{II}−imidazole complexes (*71*). The minimum path for guanidinium nitrogen hydrogen bonded to the substrate amine nitrogen is three covalent bonds and one hydrogen bond. This conclusion suggests that R160 has a role in both substrate binding and catalysis. Whether the guanidinium moiety is hydrogen bonded to the substrate hydroxyl, substrate amine, or both cannot be determined from the present data.

(4) The C1 electron spin density center on the (*S*)-2-aminopropanol- and aminoethanol-derived substrate radicals shifts away from Co^{II} by distances of 2.1 ± 0.6 and 2.1 ± 1.2 Å, respectively, in R160K relative to WT EAL. This is equivalent to the calculated 1.6 Å reduction in the length of the residue 160 side chain when arginine is replaced by lysine. The displacement is predicted to lie approximately along the Co^{II}−C1 axis (the $g_{||}$ axis of Co^{II}) by the EutB model (*5*). We therefore interpret this shift as indicating a strong Coulombic and hydrogen-bonding interaction of the positive charge on R160 with one or both substrate heteroatoms, which draws the substrate "up" in the active site in the view shown in Figure 2. The ^2H ESEEM results show that the position of the 5′-methyl center of 5′-deoxyadenosine tracks with the displacement of the radical center, because the geometry of the C1, C2, and C5′ centers in R160K and WT EAL is conserved. Therefore, we propose that a force is applied to the C5′-methyl center, which maintains the native van der Waals contact with the substrate radical center. The force on the C5′-methyl center reveals a vectoral, mechanical coupling between the protein and the radical. The force maintains the association of the C5′ center and the substrate radical at van der Waals contact during the first hydrogen atom transfer, radical rearrangement, and second hydrogen atom transfer reactions. The force must be released following HT2, so that the C5′ radical center can leave the substrate binding region and recombine with Co^{II} to re-form the Co−C bond.

ACKNOWLEDGMENT

We are grateful to Dr. Shu Feng-Jue, in the laboratory of Professor John Hepler (Department of Pharmacology, Emory University), and to Dr. Chiara Zurla and Dr. Fiorella Guerra, in the laboratory of Professor Laura Finzi (Department of Physics, Emory University), for advice and assistance with the molecular biology experiments and to Professor Diane F. Matesic (Department of Pharmaceutical Sciences, Mercer University, Atlanta) for assistance with gel electrophoresis. The use of the resources of the Cherry L. Emerson Center for Scientific Computation at Emory University (NSF CHE-0079627) is acknowledged.

SUPPORTING INFORMATION AVAILABLE

The sequences of primers used in mutagenesis studies, additional EPR simulation parameters, and ^{14}N ESEEM simulations for the Co^{II}−aminoethanol radical pair. This material is available free of charge via the Internet at http://pubs.acs.org.

REFERENCES

1. Bandarian, V., and Reed, G. H. (1999) Ethanolamine Ammonia-Lyase, in *Chemistry and Biochemistry of B12* (Banerjee, R., Ed.) pp 811−833, John Wiley and Sons, New York.
2. Toraya, T. (2003) Radical catalysis in coenzyme B-12-dependent isomerization (eliminating) reactions. *Chem. Rev. 103*, 2095–2127.
3. Bradbeer, C. (1965) Clostridial Fermentations of Choline and Ethanolamine. I. Preparation and Properties of Cell-Free Extracts. *J. Biol. Chem. 240*, 4669.
4. Faust, L. R., Connor, J. A., Roof, D. M., Hoch, J. A., and Babior, B. M. (1990) Cloning, sequencing, and expression of the genes encoding the adenosylcobalamin-dependent ethanolamine ammonia-lyase of *Salmonella typhimurium*. *J. Biol. Chem. 265*, 12462–12466.
5. Sun, L., and Warncke, K. (2006) Comparative model of EutB from coenzyme B-12-dependent ethanolamine ammonia-lyase reveals a beta(8)alpha(8), TIM-barrel fold and radical catalytic site structural features. *Proteins: Struct., Funct., Bioinf. 64*, 308–319.
6. Faust, L. P., and Babior, B. M. (1992) Overexpression, purification, and some properties of the AdoCbl-dependent ethanolamine ammonia-lyase from *Salmonella typhimurium*. *Arch. Biochem. Biophys. 294*, 50–54.
7. Mancia, F., and Evans, P. R. (1998) Conformational changes on substrate binding to methylmalonyl CoA mutase and new insights into the free radical mechanism. *Struct. Folding Des. 6*, 711–720.
8. Mancia, F., Keep, N. H., Nakagawa, A., Leadlay, P. F., McSweeney, S., Rasmussen, B., Bosecke, P., Diat, O., and Evans, P. R. (1996) How coenzyme B-12 radicals are generated: The crystal structure of methylmalonyl-coenzyme A mutase at 2 angstrom resolution. *Structure 4*, 339–350.
9. Mancia, F., Smith, G. A., and Evans, P. R. (1999) Crystal structure of substrate complexes of methylmalonyl-CoA mutase. *Biochemistry 38*, 7999–8005.

10. Reitzer, R., Gruber, K., Jogl, G., Wagner, U. G., Bothe, H., Buckel, W., and Kratky, C. (1999) Glutamate mutase from *Clostridium cochlearium*: the structure of a coenzyme B-12-dependent enzyme provides new mechanistic insights. *Structure 7*, 891–902.
11. Gruber, K., Reitzer, R., and Kratky, C. (2001) Radical Shuttling in a Protein: Ribose Pseudorotation Controls Alkyl-Radical Transfer in the Coenzyme B_{12} Dependent Enzyme Glutamate Mutase. *Angew. Chem., Int. Ed. Engl. 40*, 3377–3380.
12. Shibata, N., Masuda, J., Tobimatsu, T., Toraya, T., Suto, K., Morimoto, Y., and Yasuoka, N. (1999) A new mode of B12 binding and the direct participation of a potassium ion in enyzme catalysis: X-ray structure of diol dehydratase. *Structure 7*, 997–1008.
13. Masuda, J., Shibata, N., Morimoto, Y., Toraya, T., and Yasuoka, N. (2000) How a protein generates a catalytic radical from coenzyme B12: X-ray structure of a diol dehydratase-adeninylpentylcobalamin complex. *Structure 8*, 775–788.
14. Yaminishi, M., Yunoki, M., Tobimatsu, T., Sato, H., Matsui, J., Dokiya, A., Iuchi, Y., Oe, K., Suto, K., Shibata, N., Morimoto, Y., Yasuoka, N., and Toraya, T. (2002) The Crystal Structure of Coenzyme B_{12}-Dependent Glycerol Dehydratase in Complex with Cobalamin and Propane-1,2-Diol. *Eur. J. Biochem. 269*, 4484–4494.
15. Liao, D.-I., Dotson, G., Turner, I., Reiss, L., and Emptage, M. (2003) Crystal Structure of Substrate Free Form of Glycerol Dehydratase. *J. Inorg. Biochem. 93*, 84–91.
16. Sintchak, M. D., Arjara, G., Kellogg, B. A., Stubbe, J., and Drennan, C. L. (2002) The Crystal Structure of Class II Ribonucleotide Reductase Reveals How an Allosterically Regulated Monomer Mimics a Dimer. *Nat. Struct. Biol. 9*, 293–300.
17. Warncke, K., and Utada, A. S. (2001) Interaction of the substrate radical and the 5′-deoxyadenosine-5′-methyl group in vitamin B(12) coenzyme-dependent ethanolamine deaminase. *J. Am. Chem. Soc. 123*, 8564–8572.
18. Canfield, J. M., and Warncke, K. (2002) Geometry of reactant centers in the Co-II-substrate radical pair state of coenzyme B-12-dependent ethanolamine deaminase determined by using orientation-selection-ESEEM spectroscopy. *J. Phys. Chem. B 106*, 8831–8841.
19. LoBrutto, R., Bandarian, V., Magnusson, O. T., Chen, X., Schramm, V. L., and Reed, G. H. (2001) 5′-Deoxyadenosine contacts the substrate radical intermediate in the active site of ethanolamine ammonia-lyase: ^{2}H and ^{13}C electron nuclear double resonance studies. *Biochemistry 40*, 9–14.
20. Warncke, K. (2005) Characterization of the product radical structure in the Co(II)-product radical pair state of coenzyme B12-dependent ethanolamine deaminase by using three-pulse 2H ESEEM spectroscopy. *Biochemistry 44*, 3184–3193.
21. Canfield, J. M., and Warncke, K. (2005) Active site reactant center geometry in the Co-II-product radical pair state of coenzyme B-12-dependent ethanolamine deaminase determined by using orientation-selection electron spin-echo envelope modulation spectroscopy. *J. Phys. Chem. B 109*, 3053–3064.
22. Joint Center for Structural Genomics (2007) Crystal structure of ethanolamine ammonia-lyase heavy chain (YP_013784.1) from *Listeria monocytogenes* 4b F2365 at 2.15 Å resolution, *10.2210/pdb2qez/pdb*.
23. Babior, B. M., Moss, T. H., Orme-Johnson, W. H., and Beinert, H. (1974) The mechanism of action of ethanolamine ammonia-lyase, a B-12-dependent enzyme. The participation of paramagnetic species in the catalytic deamination of 2-aminopropanol. *J. Biol. Chem. 249*, 4537–4544.
24. Retey, J., Suckling, C. J., Arigoni, D., and Babior, B. M. (1974) The stereochemistry of the reaction catalyzed by ethanolamine ammonia-lyase, an adenosylcobalamin-dependent enzyme. *J. Biol. Chem. 249*, 6359–6360.
25. Frey, P. A. (1990) Importance of Organic Radicals in Enzymatic Cleavage of Unactivated C-H Bonds. *Chem. Rev. 90*, 1343–1357.
26. Licht, S. S., Lawrence, C. C., and Stubbe, J. (1999) Class II ribonucleotide reductases catalyze carbon-cobalt bond reformation on every turnover. *J. Am. Chem. Soc. 121*, 7463–7468.
27. Warncke, K., Schmidt, J. C., and Ke, S. C. (2008) Identification of a rearranged-substrate, product radical intermediate and the contribution of a product radical trap in vitamin B12 coenzyme-dependent ethanolamine deaminase catalysis, *J. Am. Chem. Soc.,* in press.
28. Warncke, K., Schmidt, J. C., and Ke, S. C. (1999) Identification of a rearranged-substrate, product radical intermediate and the contribution of a product radical trap in vitamin B-12 coenzyme-dependent ethanolamine deaminase catalysis. *J. Am. Chem. Soc. 121*, 10522–10528.
29. Bandarian, V., and Reed, G. H. (2002) Analysis of the electron paramagnetic resonance spectrum of a radical intermediate in the coenzyme B(12)-dependent ethanolamine ammonia-lyase catalyzed reaction of S-2-aminopropanol. *Biochemistry 41*, 8580–8588.
30. Ke, S. C. (2003) Spin-spin interaction in ethanolamine deaminase. *Biochim. Biophys. Acta 1620*, 267–272.
31. Tan, S. L., Kopczynski, M. G., Bachovchin, W. W., Orme-Johnson, W. H., and Babior, B. M. (1986) Electron spin echo studies of the composition of the paramagnetic intermediate formed during the deamination of propanolamine by ethanolamine ammonia lyase, an AdoCbl-dependent enzyme. *J. Biol. Chem. 261*, 3483–3485.
32. Ke, S. C., and Warncke, K. (1999) Interactions of substrate and product radicals with Co-II in cobalamin and with the active site in ethanolamine deaminase, characterized by ESE-EPR and N-14 ESEEM spectroscopies. *J. Am. Chem. Soc. 121*, 9922–9927.
33. Xia, L., Ballou, D. P., and Marsh, E. N. G. (2004) Role of Arg100 in the active site of adenosylcobalamin-dependent glutamate mutase. *Biochemistry 43*, 3238–3245.
34. Semialjac, M., and Schwartz, H. (2002) Computational exploration of rearrangements related to the vitamin B12-dependent ethanolamine ammonia lyase catalyzed transformation. *J. Am. Chem. Soc. 124*, 8974–8983.
35. Wetmore, S. D., Smith, D. M., Bennet, J. T., and Radom, L. (2002) Understanding the Mechanism of Action of B12-Dependent Ethanolamine Ammonia-Lyase: Synergistic Interactions at Play. *J. Am. Chem. Soc. 124*, 14054–14065.
36. Harkins, T. T., and Grissom, C. B. (1995) The Magnetic-Field Dependent Step in Bit Ethanolamine Ammonia-Lyase Is Radical-Pair Recombination. *J. Am. Chem. Soc. 117*, 566–567.
37. Ornstein, L., and Davis, B. J. (1964) Disc Electrophoresis. 1. Background and Theory. *Ann. N.Y. Acad. Sci. 121*, 321–349.
38. Laemmli, U. K. (1970) Cleavage of structural proteins during the assembly of the head of bacteriophage T4. *Nature 227*, 680–685.
39. Kaplan, B. H., and Stadtman, E. R. (1968) Ethanolamine deaminase, a cobamide coenzyme-dependent enzyme. I. Purification, assay, and properties of the enzyme. *J. Biol. Chem. 243*, 1787–1793.
40. Holloway, M. R., White, H. A., Joblin, K. N., Johnson, A. W., Lappert, M. F., and Wallis, C. O. (1978) A spectrophotometric rapid kinetic study of reactions catalyzed by coenzyme B12-dependent ethanolamine ammonia-lyase. *Eur. J. Biochem. 82*, 143–154.
41. Cornish-Bowden, A. (1981) *Fundamentals of enzyme kinetics*, Butterworths, Boston, MA.
42. Hollaway, M. R., Johnson, A. W., Lappert, M. F., and Wallis, O. C. (1980) The number of functional active sites per molecule of the adenosylcobalamin-dependent enzyme, ethanolamine ammonia-lyase, as determined by a kinetic method. *Eur. J. Biochem. 111*, 177–188.
43. Bandarian, V., and Reed, G. H. (1999) Hydrazine cation radical in the active site of ethanolamine ammonia-lyase: mechanism-based inactivation by hydroxyethylhydrazine. *Biochemistry 38*, 12394–12402.
44. Britt, R. D., and Klein, M. P. (1987) A Versatile Loop Gap Resonator Probe for Low-Temperature Electron Spin-Echo Studies. *J. Magn. Reson. 74*, 535–540.
45. Lin, C. P., Bowman, M. K., and Norris, J. R. (1985) A Folded Half-Wave Resonator for Electron-Spin-Resonance Spectroscopy. *J. Magn. Reson. 65*, 369–374.
46. Dikanov, S. A., and Tsvetkov, Y. D. (1992) *Electron Spin Echo Envolop Modulation (ESEEM) Spectroscopy*, CRC Press, Boca Raton, FL.
47. Deligiannakis, Y., Louloudi, M., and Hadjiliadis, N. (2000) Electron spin echo envelope modulation (ESEEM) spectroscopy as a tool to investigate the coordination environment of metal centers. *Coord. Chem. Rev. 204*, 1–112.
48. Jeschke, G., and Schweiger, A. (2001) *Principles of Pulse Electron Paramagnetic Resonance*, Oxford University Press, New York.
49. Fauth, J. M., Schweiger, A., Braunschweiler, L., Forrer, J., and Ernst, R. R. (1986) Elimination of Unwanted Echoes and Reduction of Dead Time in 3-Pulse Electron Spin-Echo Spectroscopy. *J. Magn. Reson. 66*, 74–85.
50. Fauth, J. M., Schweiger, A., and Ernst, R. R. (1989) Recovery of Broad Hyperfine Lines in Electron Spin-Echo Envelope Modulation Spectroscopy of Disordered-Systems. *J. Magn. Reson. 81*, 262–274.

51. Hyde, J. S., Rist, G. H., and Eriksson, L. E. (1968) Endor of Methyl Matrix and Alpha Protons in Amorphous and Polycrystalline Matrices. *J. Phys. Chem. 72*, 4269.
52. Mims, W. B. (1972) Envelope Modulation in Spin-Echo Experiments. *Phys. Rev. B: Solid State 5*, 2409.
53. Mims, W. B., and Peisach, J. (1989) *Advanced EPR: Appications in Biology and Chemistry* (Hoff, A. J., Ed.) pp 1−57, Elsevier, New York.
54. Mims, W. B., Davis, J. L., and Peisach, J. (1990) The Exchange of Hydrogen Ions and of Water Molecules near the Active Site of Cytochrome c. *J. Magn. Reson. 86*, 273–292.
55. Eaton, S. S., More, K. M., Sawant, B. M., Boymel, P. M., and Eaton, G. R. (1983) Metal Nitroxyl Interactions. 29. Electron-Paramagnetic-Res Studies of Spin-Labeled Copper-Complexes in Frozen Solution. *J. Magn. Reson. 52*, 435–449.
56. Boas, J. F., Hicks, P. R., Pilbrow, J. R., and Smith, T. D. (1978) Interpretation of Electron Spin Resonance Spectra Due to Some B12-dependent Enzyme Reactions. *J. Chem. Soc., Faraday II 74*, 417–431.
57. Pilbrow, J. R. (1982) EPR of B12-dependent enzyme reactions and related systems, in *B12* (Dolphin, D., Ed.) Vol. 1, pp 431−462, Wiley, New York.
58. Mims, W. B. (1972) Amplitudes of Superhyperfine Frequencies Displayed in Electron-Spin Echo Envelope. *Phys. Rev. B: Solid State 6*, 3543.
59. Dikanov, S. A., Shubin, A. A., and Parmon, V. N. (1981) Modulation Effects in the Electron-Spin Echo Resulting from Hyperfine Interaction with a Nucleus of an Arbitrary Spin. *J. Magn. Reson. 42*, 474–487.
60. Hellwege, K.-H., and Hellwege, A. M. (1988) *Landolt-Bornstein Numerical Data and Functional Relationships in Science and Technology*, Vol. A, Springer-Verlag, New York.
61. Mims, W. B., and Peisach, J. (1989) ESEEM and LEFE of metalloproteins and model compounds, in *Advanced EPR: Applications in Biology and Chemistry* (Hoff, A. J., Ed.) pp 1−57, Elsevier, New York.
62. Press, W. H., Teukolsky, S. A., Vetterling, W. T., and Flannery, B. P. (1992) *Nemerical Recipes in C: The Art of Scientific Computing*, 2nd ed., Cambridge University Press, New York.
63. Lagarias, J. C., Reeds, J. A., Wright, M. H., and Wright, P. E. (1998) Convergence Properties of the Nelder-Mead Simplex Method in Low Dimensions. *SIAM J. Optimization 9*, 112–147.
64. (1981) CERN Program Library, D506 MINUIT, Function Minimization and Error Analysis, Geneva.
65. Kim, J., Mao, J., and Gunner, M. R. (2005) Are acidic and basic groups in buried proteins predicted to be ionized? *J. Mol. Biol. 348*, 1283–1298.
66. Fersht, A. (1999) *Structure and Mechanism in Protein Science*, W. H. Freeman and Co., New York.
67. Gerfen, G. J. (1999) EPR spectroscopy of B12-dependent enzymes, in *Chemistry and Biochemistry of B12* (Banerjee, R., Ed.) pp 165−195, John Wiley and Sons, New York.
68. Wertz, J. E., and Bolton, J. R. (1986) *Electron Spin Resonance*, Chapman and Hall, New York.
69. Bandarian, V., and Reed, G. H. (2000) Isotope effects in the transient phases of the reaction catalyzed by ethanolamine ammonia-lyase: Determination of the number of exchangeable hydrogens in the enzyme-cofactor complex. *Biochemistry 39*, 12069–12075.
70. Flanagan, H. L., and Singel, D. J. (1987) Analysis of ^{14}N ESEEM Patterns of Randomly Oriented Solids. *J. Chem. Phys. 87*, 5606–5616.
71. Mims, W. B., and Peisach, J. (1978) Nuclear Modulation Effect in Electron-Spin Echoes for Complexes of Cu^{2+} and Imidazole with N-14 and N-15. *J. Chem. Phys. 69*, 4921–4930.
72. Edmonds, D. T. (1977) Nuclear Quadrupole Double Resonance. *Phys. Lett. C 29*, 233–290.
73. Safin, I. A., and Osokin, D. Y. (1977) *Nuclear Quadrupole Resonance in Nitrogen Compounds*, pp 181−250, Science, Moscow.
74. Heller, C., and McConnell, H. M. (1960) Electron-nuclear interactions through hyperconjugation. *J. Chem. Phys. 32*, 1535–1539.

BI702366E